CHARACTERIZATION OF BENDING STIFFNESS AND SPONTANEOUS BUCKLING OF ALPHA-HELICES AND COILED COILS

A Thesis

by

SIRISH KAUSHIK LAKKARAJU

Submitted to the Office of Graduate Studies of
Texas A&M University
in partial fulfillment of the requirements for the degree of

MASTER OF SCIENCE

August 2008

Major Subject: Biomedical Engineering

CHARACTERIZATION OF BENDING STIFFNESS AND SPONTANEOUS BUCKLING OF ALPHA-HELICES AND COILED COILS

A Thesis

by

SIRISH KAUSHIK LAKKARAJU

Submitted to the Office of Graduate Studies of
Texas A&M University
in partial fulfillment of the requirements for the degree of

MASTER OF SCIENCE

Approved by:

Chair of Committee,	Wonmuk Hwang
Committee Members,	Mariappan Muthuchamy
	Roland Kaunas
Head of Department,	Gerard Cote

August 2008

Major Subject: Biomedical Engineering

ABSTRACT

Characterization of

Bending Stiffness and Spontaneous Buckling

of Alpha-Helices and Coiled Coils. (August 2008)

Sirish Kaushik Lakkaraju, B.En., University of Madras, India

Chair of Advisory Committee: Dr.Wonmuk Hwang

Elasticity of α-helices and coiled coils have often been described by a linear response to local bending with bending stiffness (K_b) and persistence length (L_p) describing their flexibility. However, we observed that the non-bonded forces along the length of these structures are not screened at physiological conditions and introduce a buckling instability. For α-helical systems of same composition, but different lengths, this is identified by a drop in K_b for longer helices and the length where this drop is triggered is referred to as the critical buckling length. When shorter than their critical buckling length they behave linearly, and K_b calculated using normal mode analysis in this regime is about $(3.0 - 3.4) \times 10^{-28}$ Nm^2 for α-helices with varying compositions, and about $(1.9 - 2.1) \times 10^{-27}$ Nm^2 for coiled coils with leucine zipper periodicity. Beyond the critical buckling length, normal mode solutions turn imaginary, leading to an eventual disappearance of bending modes. Investigations with one dimensional (1-D) linear chains of beads (a simplistic representation of bio-filaments) show that non-bonded forces have a reciprocal relation with the critical buckling length (no buckling instability existed in the absence of non-bonded forces). Critical buckling length is 115.3 ± 2.9 Å for α-helices and 695.1 ± 44.8 Å for coiled coils with leucine zipper periodicity, which is much smaller than their L_p ($\sim$ 800 Å for α-helices and $\sim$ 3000 Å for coiled coils).

To Bhagwan Sri Sathya Saibaba

ACKNOWLEDGMENTS

I would like to thank my committee chair, Dr. Wonmuk Hwang, for his patience, guidance and support throughout the course of this research.

I extend my deep gratitude to Dr. Roland Kaunas and Dr. Mariappan Muthuchamy for serving on my committee and providing valuable suggestions.

I thank Jiyong Park for his input at various junctures of this project.

I thank Dr. Gerald Offer for his C code that has been used to build the coiled coils in this work.

Finally, I also thank my friends here at College Station for making my stay here a wonderful experience.

TABLE OF CONTENTS

Page

LIST OF FIGURES

FIGURE Page

CHAPTER I

INTRODUCTION

Alpha-helices formed by a hydrogen bonding between i and $(i+4)$th amino acids [1] and their supra molecular assemblies like coiled coils [2] have important mechanical roles. For instance, vesicle bound soluble N-ethylmaleimide-sensitive factor (NSF) attachment receptors (SNAREs) are α-helical proteins that are used to dock the vesicles at the membrane [3]. Flexibility of the coiled coil neck in the kinesin motor controls its stalling force and load bearing capacity [4], while tropomyosin's sliding on actin controls actin-myosin interactions towards muscle contraction [5]. Accurate characterization of their mechanical properties through systematic studies of deformation and structural dynamics is hence important towards building reliable models that decipher macroscopic phenomena on a microscopic scale [6].

Most of the experimental [7] and computational [8] [9] studies in the past have treated these structures as linearly elastic homogeneous rods [10]. This is based on the observation that some of the common non-bonded interactions like hydrogen bonding in α-helices and knob into hole packing [2] in coiled coils of varying compositions, give these structures their stiffness [8] [11] [12] [13] [14] [15].

However, we observe that the intrinsic non-bonded interactions also introduce a buckling instability that is characterized by the length of the system. On measuring bending stiffness (K_b) of α-helices of different lengths, we see that there is a drop in K_b for longer helices. Investigations reveal that this drop is due to the predominance of non-bonded forces in longer systems. We call the length scale where this predominance starts, the critical buckling length. Coiled coils and a one-dimensional

---

The journal model is *IEEE Transactions on Automatic Control*.

(1-D) linear chains (built as a representative of filamentous proteins) also exhibit this buckling instability.

In this work, we have determined K_b for α-helices and coiled coils of varying sizes and compositions from the vibrational frequencies of their normal bending modes using the wave theory of rods. We have also calculated their critical buckling length, which is governed by the magnitude of non-bonded forces present in such systems. For all calculations, we treat α-helices and coiled coils as flexible cylindrical rods. When shorter than their critical buckling length and long enough to have a good aspect ratio (typically lesser than 0.1), bending stiffness for α-helices of different compositions vary in the range of $(2.985-3.356)\times10^{-28}$ Nm^2 (in agreement with previous studies [8] [9]). Bending stiffness for long coiled coils (longer than 160 Å and shorter than 700 Å) with leucine zipper periodicity varies between $(1.883 - 2.107) \times 10^{-27}$Nm^2. This is higher than previous observed bending stiffnesses of coiled coils [9] [16], but we attribute this to the tighter knob into hole packing [2] by the unbroken heptad repeat sequence in a leucine zipper, which is uncommon in other coiled coils.

Buckling instability due to the non-bonded forces is also seen in the 1-D linear beads on a chain system. Persistence length from the worm like chain (WLC) model calculations (thermal fluctuations of end atoms) also dropped beyond its critical buckling length.

While buckling instability is an outcome of our calculations of bending stiffness using frequencies of the normal bending modes of rods of different lengths, we correlate and compare these results with thermal fluctuation studies of 1-D linear chains and force displacement analysis of coiled coils. The thesis is organized as follows: Theory and Computational Methods section discuss the methodology behind using these techniques for calculating bending stiffness. In the Results section, we analyze bending stiffness variation as a function of the length and subsequently calculate

the critical buckling length of α-helices, coiled coils and 1-D linear chains. We then conclude by discussing the relevance of these findings towards naturally occurring α-helices and coiled coils.

CHAPTER II

METHODOLOGY

In the Theory section, the various methods used for calculation of bending stiffnes are discussed. Details of the computational steps involved are then discussed in the Computational Steps section.

A. Theory

1. Normal Mode Analysis (NMA)

Normal modes represent different types of low frequency vibrational motion. In a chain, these are seen as bending, stretching and torsion of a structure. When α-helices, coiled coils and 1D linear chains are treated as cylindrical rods (Fig.1), the frequencies of motion from NMA can be used to calculate the mechanical stiffness coefficients using the wave equations of a thin rod. For a freely vibrating rod in a linear elastic regime, the bending stiffness can be retrieved from the following relation,

$$K_b^{(n)} = \frac{\rho_l (\omega^{(n)})^2}{(k^{(n)})^4} \tag{2.1}$$

where ρ_l is the mass per unit length (kg/m), $K_b^{(n)}$ is the bending stiffness from mode n ($\mathrm{N}m^2$), $\omega^{(n)}$ is the angular frequency of the n-th bending mode (obtained from $2\pi \times 3 \times 10^{10} \times f$ where f is bending frequency in cm^{-1}), $k^{(n)}$ is the wave number given by $\frac{c^{(n)}}{L}$ such that $c^{(1)} = 4.7300$, $c^{(2)} = 7.8532$, $c^{(3)} = 10.9956$, L is the length of the rod [9] [17]. In an ideal linear elastic system, bending stiffness of any mode $K_b^{(n)}$ should be equal to each other and can be represented as K_b.

Intrinsically present non-bonded force (F_{nb}) however, introduce a buckling instability that is observed to be compressive. Incorporating this into the wave theory of

rods, it can be shown that [18],

$$(\omega^{(n)})^2 L^2 = \frac{K_b^{(n)}(c^{(n)})^4}{\rho_l L^2} - F_{nb}(c^{(n)})^4 \tag{2.2}$$

In Eqn. 2.2, when $F_{nb} \geq K_b^{(n)}(k^{(n)})^2$, $\omega^{(n)}$ becomes imaginary, leading to two normal mode solutions that increase and decrease exponentially with time. Since $k^{(n)} \sim L^{-1}$, for a given F_{nb}, there exists a critical buckling length ($L_c^{(n)}$),

$$L_c^{(n)} = c^{(n)}\sqrt{\frac{K_b^{(n)}}{F_{nb}}} \tag{2.3}$$

such that for $L > L_c^{(n)}$, spontaneous buckling at mode n occurs. This is observed by the decrease in "apparent" bending stiffness when Eqn. 2.1 is used to analyze the data.

From Eqn. 2.2, there exists only a limited length scale determined by the condition $K_b^{(n)}(k^{(n)})^2 > F_{nb}$, where in the wave propogation is possible.

2. Thermal Motion Analysis (TMA)

We use a 1-D linear chain of beads (Fig.1(c)) because of its simple geomety and because it is easier to control the non-bonded interactions between atoms. Persistence length(L_p) of this chain can be from the end to end distances using the WLC model.

$$< R^2 >= 2L_p(L + L_p(e^{\frac{-L}{L_p}} - 1)) \tag{2.4}$$

where $< R^2 >$ is the ensemble average of the square of end to end distance (Å^2) and L is the length of the chain (Å) [19]. By subjecting the chain to thermal undulations at 300 K, we can determine its L_p from the distance between the end atoms using the above relation. L_p is directly related to K_b,

$$L_p = \frac{K_b}{kT} \tag{2.5}$$

where k is the Boltzmann constant (Nm/K) and T is the temperature (K). K_b so retrieved from L_p, is comparable to $K_b^{(n)}$ measured using NMA, decreasing for 1-D chains longer than their $L_c^{(1)}$.

3. Steered Molecular Dynamics (SMD)

A cantilevered rod subjected to a transverse force, undergoes a displacement given by the relation,

$$F = 3K_b \frac{\triangle y}{L^3} \tag{2.6}$$

where F is the transverse force (pN), $\triangle y$ is the vertical displacement (Å) and L is the length of the rod (Å). For a rod of length L, K_b can thus be retrieved from the lateral stiffness ($k_\perp$) which is the slope of the force displacement curve (F vs $\triangle y$) plotted by restraining one end of the rod and applying the transverse force at the free end using the relation [17],

$$k_\perp = \frac{F}{\triangle y} = \frac{3K_b}{L^3} \tag{2.7}$$

B. Computational Methods

Simulations were carried out using CHARMM versions c3b1 and c34b1, where the param19 force field was used. Visual Molecular Dynamics (VMD) [20] was used for visualizations.

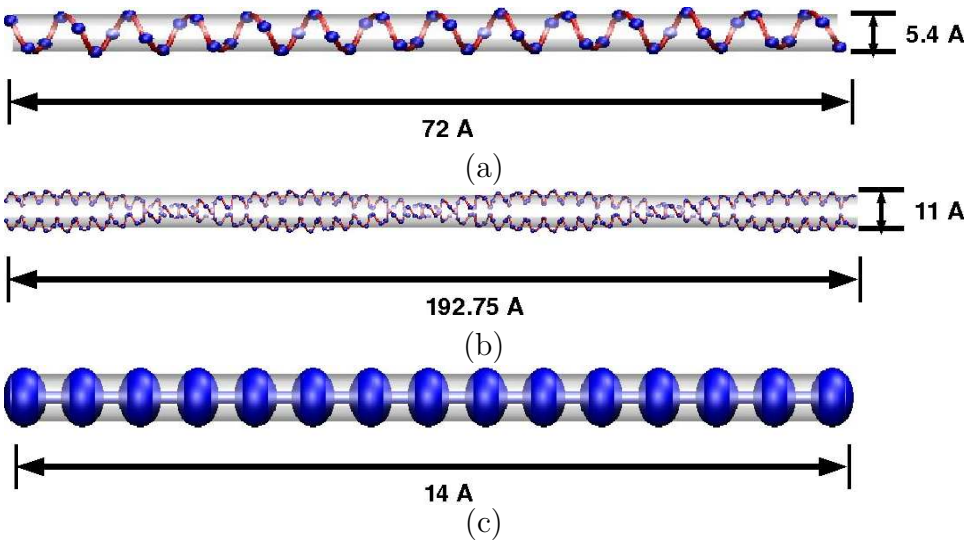

Fig. 1. Cylindrical rod representation. Examples of α-helices, coiled coils and the 1-D linear chains that are treated as flexible cylindrical rods for calculating bending stiffness using the wave theory rods. (a) Poly-Alanine α-helix. (b) Coiled coil with leucine zipper periodicity. (c) 1-D chain.

1. Alpha-helices

a. Helix construction

Alpha-helices of alanine, glycine, leucine and with compositions of helical segments randomly chosen from a single α-helical chain of tropomyosin were constructed with the following set of dihedral angles:

$$\phi = -57°, \psi = -47° \text{ and } \omega = 180°$$

where ϕ, ψ and ω are the principal torsion angles describing the rotation about $N - C_\alpha$, $C_\alpha - C$, and $C - N$ axes, respectively [21]. This ω is different from $\omega^{(n)}$, which is the vibrational frequency of bending mode n.

b. NMA

1. Minimization : NMA needs a molecule to have the lowest energy conformation. The helix is hence minimized with an initial 800 steps of Steepest Descent (SD) and then a large number of Adopted Basis Newton Raphsons (ABNR) minimization steps, with a predefined tolerance limit as the exit criteria. SD, the simplest of all minimization procedures is used in moving the system towards a minimum, removing the bad contacts and avoiding an unreasonably high energy configuration. It is however inefficient for attaining a local minimum and hence the number of steps are limited to 800. ABNR on the other hand, calculates a residual gradient vector at each step by applying the Newtons Raphsons algorithm on the subspace of the co-ordinate vector (spanned by the displacement co-ordinates of the last positions). Minimization iterations end when the Root Mean Square of the Gradient (GRMS) reaches the tolerance limit. The helical structures remained intact with hydrogen bonding distance between residues i and $i+4$ being about 2.03 Å after minimization.

2. Heating & Equilibration: In Molecular Dynamics, random velocities are initially assigned from a Maxwell distribution to each of the atoms in the molecule. This random assignment does not allocate correct velocities and the system is not at thermodynamic equilibrium. To achieve this equilibrium, velocities are rescaled over a number of steps till the total kinetic energy of the system becomes constant. The rescaling of the velocities can be dictated by a temperature, since the absolute temperature is related to the mean kinetic energy,

$$T = \frac{2}{2Nk} \sum \frac{m_i |\vec{v}_i|^2}{2} \tag{2.8}$$

where N is the number of atoms, m_i and v_i are the mass and velocities of the i-th

atom and k is the Boltzmann constant. Heating can thus be achieved in a thermodynamic equilibrium, by multiplying all atom velocities with $\sqrt{\frac{T_{desired}}{T_{current}}}$ [22]. Prior to retrieving the vibrational bending frequencies, the minimized α-helices were thus heated from 0 to 100 K for a period of 50 ps. Equilibration was then carried out for 20 ps at 100 K. Alpha-helices so heated and equilibrated are further minimized following the procedure in 1 to ensure that the molecule had a low energy conformation along with relaxed side chains. The hydrogen bonding distance between i and $i+4$ residues remained at about 2.03 Å, with no notable deformation in the structure.

3. Vibrational Analysis : CHARMM subroutine VIBRA, was used for retrieving the vibrational frequencies of the first 100 modes. Six lowest modes reported by VIBRA are global translations and rotations along the center of mass and are discarded [23]. The first bending mode hence occurs at mode 7 of the VIBRA output.

2. Coiled coils

a. Coiled coil construction

Coiled coils of different lengths were constructed using leucine zipper sequence periodicity. Naturally occurring leucine zipper has 31 residues per chain with Arginine (not a part of the heptad repeats) as the first residue [24]. We used the 28 residues (unbroken heptad repeats) that follow Arginine as the leucine zipper period (residues per chain in a single letter format:MKQLEDKVEELLSKNYHLENEVARLKKL). With leucine zipper periods as the sequence of a single α-helical chain, two stranded parallel coiled coil rods were built using a C program provided by Offer [25]. Two parallel α-helices of such leucine zipper periodicity with an axial translation of 1.495 Å were

intertwined with a relative orientation of 210^o, to form a super helix with a major helical radius of 4.7 Å and a pitch of 144 Å [25]. Backbone of the coiled coil built this way aligned well with the backbone of a naturally occurring crystal structure of leucine zipper (Root Mean Square Deviation (RMSD) 0.01 Å). This crystal structure is downloaded from the Protein Data Bank (PDB code:2ZTA). The side chains however, had an RMSD of about 1.1 Å. To have a good knob into hole packing, the side chains co-ordinates in the long rods built using the C code, were replaced by those from the crystal structure.

We determined K_b of straight coiled coils without the inherent bend found in some of the naturally occurring coiled coils [26] since the equations from the wave theory of rods (Eqn. 2.1, Eqn. 2.2) used to determine the bending stiffness are not well described for bent cylindrical rods [18]. Determining K_b by considering slightly bent coiled coils as straight cylinders [9] introduce length driven errors and lead to an under estimation of the actual value. Despite considering limited cases of straight coiled coils with leucine zipper periodicity, bending stiffness and critical buckling length thus calculated can be considered a generic estimate for naturally occurring coiled coils. For instance, the backbone of a coiled coil with 101 residues of leucine zipper periodicity per chain has an RMSD of 0.1 Å with the backbone chain of an actin bundling cortexillin (101 residues per chain) [27], showing a good geometric resemblance. Bending stiffness calculated for these structures are similar ($K_b^{(1)} \simeq 1.759 \times 10^{-27}$ Nm^2 for cortexillin, versus 1.683×10^{-27} Nm^2 for leucine zipper coiled coil of the same size).

For all coiled coils simulations, the analytical continuum solvent potential (ACE2) [28] was used to incorporate the solvent effects on atoms in the structure. The constants used in this technique are SEPS = 80 (dielectric constant of the solvent), IEPS = 1 (dielectric constant of the protein) and ALPHA = 1.3 (a factor that controls the width

of the Gaussian density distributions describing the volumes occupied by individual atoms). Without ACE2 providing the solvent environment, strong electrostatic interactions between the charged side chains across the hydrophilic face of a coiled coil in vacuum would denature the structure.

Length of a Coiled Coil. We calculated the length of the 2 stranded coiled coils in the following way. CHARMM command, COOR HELIX determines the helical axis for a given set of atoms. The output also defines the beginning and end positions for this helical axis vector. Using this, we first define two points at the N terminus of the coiled coil from the begin position vectors of the helical axes for the first 10 C_α atoms in each of the two α-helical chains of the coiled coil (call them b1 and b2 for chain 1 and 2, respectively). We then define two points at the C-terminal of the coiled coil from the end position vectors of the helical axes for last 10 C_α atoms at the C-terminal of each chain (call them e1 and e2 for chain 1 and 2, respectively). Defining the lines connecting b1 & b2 as b1b2 and e1 & e2 as e1e2, the length of the coiled coil is then calculated as the distance between the midpoints of b1b2 and e1e2 (Fig.2).

b. NMA

1. Minimization : Coiled coils are subjected to a two step minimization process. First, the side chains are allowed to relax using the minimization technique discussed in α-helices (Ref. α-helices NMA step. 1), after harmonically restraining the backbone chain (C_α-C-N atoms) with a mass weighed force constant of 5 kcal/molÅ^2. Subsequently, the harmonic constraints are removed and the whole structure is again minimized using the same α-helix minimization procedure (Ref. α-helices NMA step. 1).

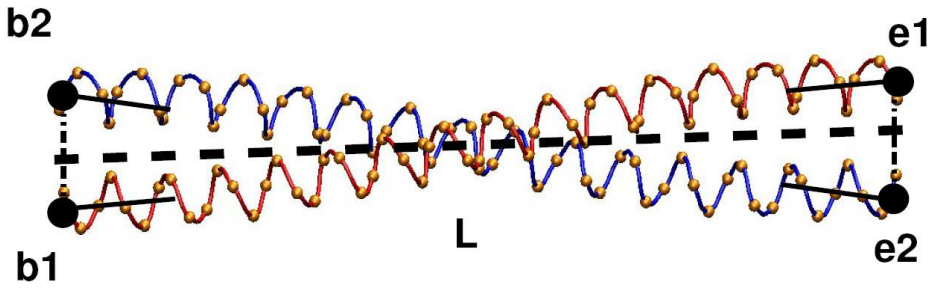

Fig. 2. Calculation of the length of a coiled coil. Shown here is an 80.48 Å coiled coil with leucine zipper periodicity. The little black lines along the individual α-helical chains represent the helical axes of the first and last 10 C_α atoms in that chain. The exaggerated black spots represent the points obtained using COOR HELIX command that give us the start and end positions of the helical axis. The length of the coiled coil, L is thus the length of the dashed line joining the midpoints of b1b2 and e1e2.

The coiled coils were then heated and equilibrated followed by a second minimization as with α-helices. However, no significant difference in the backbone (RMSD $\simeq$ 0.008 Å, measured for a 80.3 Å coiled coil) and the side chain orientation (RMSD 1.1 Å) is observed before and after the heat cycle. Also, bending stiffness ($K_b^{(1)}$) of structures that were just minimized, and that of structures subjected to heating, equilibration and a second minimization after the initial minimization were similar (1.152×10^{-27} Nm^2, for only minimized and 1.178×10^{-27} Nm^2 for minimized, heat and re-minimized coiled coil of 80.3 Å). Further, coiled coils that were energy minimized only, without a heat cycle, have a good side chain packing and alignment (RMSD of the side chains 0.5 Å) with the structures predicted using the SCWRL package [29]. Hence, we report NMA results of structures that were simply minimized till they reached a low energy conformation.

2. Vibrational Analysis: Vibrational bending frequencies were then retrieved using the VIBRA command mentioned in α-helices NMA step 3.

c. SMD

1. Minimization: The same steps of minimization are applied here, as discussed in coiled coils NMA step 1.

2. Heating: The coiled coil rods were heated from 0 to 300 K for 30 ps, by increasing the temperature at a rate of 10 K every 1 ps (a tolerance window of $\pm$10 K). During heating, the backbone heavy atoms of the individual α-helices were harmonically constrained with a mass weighed force constant of 5kcal/mol$\mathring{A}^2$ to prevent thermal unwinding. Subsequently, the heat cycle continued for another 230 ps at 300 K.

3. Equilibration: After heating, the harmonic restraints were taken off, and the coiled coil rods were equilibrated at 300K for another 500ps, with tolerance limits of $\pm$10 K.

4. Force Dynamics: The first four N terminal C_α atoms of coiled coils aligned parallel to the x-axis (using COOR ORIE) are restrained and point forces were applied along the y-axis at the C terminal C_α atom. For a 162.35 Å coiled coil, point force of 3,4,5 and 6 pN were each applied to the equilibrated structures for 2ns. For a 244.82 Å coiled coil, 0.5, 1, 1.5 and 2 pN point forces were each applied to the equilibrated structures for 4 ns. Subsequently, the time averaged displacement of the cantilevered rods is measured and force displacement curves are plotted.

3. 1D chain model

1-D linear chains of varying lengths containing beads(atoms) of same mass (mass of a carbon atom), zero charge, uniform bond strength, same van der Waals potential and radius were built for NMA and TMA analysis.

a. NMA

Same steps as that applied for NMA of α-helices were followed for the 1-D chain. Minimization is needed for the structures to attain an equilibrium distance between the beads (bond length between the atoms) for cases of a non-zero van der Waal's potential in each bead (atom). For instance, in a 1-D chain with linear bond strength of 4000 kcal/mol, angular bond strength of 400 kcal/mol rad^2 and a non-bonded potential of -440 kcal/mol at a van-der Waals radius of 2 Å between atoms, the bond length reduced from 1 Åto about 0.993 Åafter minimization.

b. TMA

1. Minimization: Same minimization treatment as applied for α-helices (Ref.α-helix minimization procedure).

2. Heating & Equilibration: 1D chains were heated from 0 K to 300 K in 60 ps by increasing the temperature by 5 K every 1 ps. The heat cycle is continued for another 40 ps at 300 K(tolerance of $\pm$5 K). This was followed by another 400 ps of equilibration at 300K(tolerance limits of $\pm$5 K).

3. Production run: 1D chains so heated and equilibrated, were subjected to several hundred nanoseconds of production run at 300K using Langevin Dynamics which mimics the viscous aspect of a solvent by incorporating a frictional coefficient usually set to 50 ps^{-1}. Importantly, Langevin dynamics allow controlling

the temperature of the system like a thermostat [30] maintaining the 1-D chain at 300 K with a tolerance of ± 5 K. Motion of the chain due to thermal undulations is a random process such that the time averaged distance vector between the end atoms should be zero. The time scale over which this condition is satisfied, increases as the length of the chain increases. Once the time averaged distance vector between the end atoms is zero, the average of the square of the distance vector between the end atoms in time is obtained for L_p measurements. The root mean square of the center of mass vector for the linear chain over the complete time scale of the production run varies linearly with time, confirming that the chain follows a diffusion path.

CHAPTER III

RESULTS

In this chapter, we discuss the results of the NMA, TMA and SMD tests on α-helices, coiled coils and 1-D chains and their significance.

A. Results

1. Bending stiffness curve

We determined the bending stiffness of α-helices, coiled coils and 1-D linear chains of different lengths, and plotted $K_b^{(n)}$ as a function of their length. Ideally, if these structures were homogeneous and linearly elastic, the curve tracing $K_b^{(n)}$ at various lengths (bending stiffness curve) should be a horizontal line. However, $K_b^{(n)}$ calculated using NMA,TMA or SMD for all of the above mentioned structures is a constant only for a limited length scale. Very short structures, for example α helices with lengths between 30 and 70 Å have a high aspect ratio (a practical limit of 1/10 is defined by Go [31]) and hence do not satisfy the basic requirement of the wave theory of rods. Also, energy contribution due to van der Waals and other non-bonded interactions between the end atoms of the structure are non-trivial for short helices. Hence, the calculated $K_b^{(n)}$ is smaller (by about 20%) than that for longer structures. The drop in $K_b^{(n)}$ for longer lengths however, is attributed to the effect of non-bonded interactions that persist along the length of the structure. The point along the bending stiffness curve, where this drop in $K_b^{(n)}$ is triggered, is identified as the critical buckling length ($L_c^{(n)}$) and its characterization is discussed in the next section (X-Y plots). Discussed below is the bending stiffness curve for each of the mentioned structures.

a. Alpha-helix

$K_b^{(n)}$ for various lengths is calculated by plugging the characteristic vibrational frequencies of the n-th bending mode into Eqn. 2.1. When the aspect ratio is greater than 0.1 (short helices 30∼70 Å), $K_b^{(n)}$ is smaller ($2.219 \times 10^{-28} - 2.779 \times 10^{-28}$ Nm^2). In the horizontal phase of the bending stiffness curve for poly-alanine (70∼100 Å for $K_b^{(1)}$, 70∼215 Å for $K_b^{(2)}$ and 70∼295 Å for $K_b^{(3)}$), $K_b^{(1)}$ ($(2.985 - 3.013) \times 10^{-28}$Nm^2), $K_b^{(2)}$ ($(3.107 - 3.210) \times 10^{-28}$ Nm^2)& $K_b^{(3)}$ ($(3.243 - 3.401) \times 10^{(-28)}$Nm^2) are similar and in agreement with previous computational studies [8] [9]. Hence, NMA is a reliable technique for retrieving bending stiffness of a structure and within the horizontal phase, bending stiffness can be calculated using vibrational frequencies from any of the bending modes. As expected, the point along the curve, where bending stiffness drops, identified as $L_c^{(n)}$, increased for higher modes ($L_c^{(1)} \simeq 100$ Å, $L_c^{(2)} \simeq 190$ Å & $L_c^{(3)} \simeq 310$ Å). $L_c^{(n)}$ from these curves are an estimate and for a more accurate characterization we use Eqn. 2.2 (Ref. Sec. 2).

Discussed below are the effects of amino acid composition, backbone hydrogen bonding, surrounding medium and the cut-off distance on the stiffness of an α-helix. Bending stiffness curves are plotted by varying each of these parameters.

1. Amino acid composition - $K_b^{(1)}$ from different lengths of α-helices built of varying compositions like poly-alanine (highest helix forming propensity), poly-glycine (no side chain), poly-leucine and with sequences from tropomyosin show that bending stiffness is relatively independent of sequence composition of an α-helix (Fig.3(a)). This is in agreement with earlier computational [8], [9] and experimental [23] studies that point towards hydrogen bonding controlling the bending stiffness of an α-helix.

2. Backbone hydrogen bond strength - The hydrogen bond strength for a 50 residue

poly-alanine α-helix was changed by controlling the electrostatic force between the O^- and the H^+ atoms in the backbone chain's C=O and N-H network. From Fig.3(b), bending stiffness varies proportionally with the hydrogen bond strength. Hence, hydrogen bonding indeed controls the bending stiffness of an α-helix [12]. Interestingly, when the electrostatic force between the O^- and H^+ atoms is made zero (retaining the van der Waal's interactions), bending stiffness is non-zero ($K_b^{(1)} \simeq 1.441 \times 10^{-28} Nm^2$). The structure did not experience any denaturation on minimization, and the length of the hydrogen bond was about 2.3 Å (under normal hydrogen bonding this is about 2.03 Å). This shows that apart from electrostatic interactions, van der Waal's interactions between O^- and H^+ atoms in the hydrogen bonding and the non-bonded interactions between other atoms also contribute significantly towards the stiffness of an α-helix.

3. Surrounding medium - RDIE is a distance dielectric algorithm, which incorporates the permittivity of the surrounding medium (dielectric constant) into energy calculations between two atoms. By setting the dielectric constant(ϵ) to 80, we artificially create an environment of water between the atoms of the α-helix. α-helices are observed to be softer in RDIE. $K_b^{(2)}$ for poly-alanine α -helices between 70 and 100 Å in RDIE is about $(3.107 - 3.210) \times 10^{-28}$ Nm^2, whereas in vacuum its about $(5.109 - 5.606) \times 10^{-28}$ Nm^2 (Fig.3(c)). This is due to the fact that water reduces the electrostatic interactions and hence the hydrogen bonding force between atoms in the helix, making the α-helix less stiff.

4. Cut-off distance for non-bonded interactions - Bending stiffness curves from varying the hydrogen bond strength and surrounding medium show that non-

bonded interactions play an important role in controlling the stiffness of α-helices. Typically, interactions between atoms greater than 12 Å away are treated negligible and not considered in energy calculations. However, we decided to consider the interactions between all atoms by increasing this cut off distance to infinity and see its effect on $K_b^{(n)}$ at varying lengths of poly-Alanine α-helix. While bending stiffness ($K_b^{(1)}$ & $K_b^{(2)}$) from the infinite cut-off calculations are comparable to that calculated when cut-off is 12 Å in the horizontal region ($K_b^{(2)} \simeq (3.104 - 3.115) \times 10^{-28}$ Nm^2 for infinite cut-off, $K_b^{(2)} \simeq (3.107 - 3.210) \times 10^{-28}$ Nm^2 for a cut-off of 12 Å), the drop in bending stiffness triggered for shorter helices ($L_c^{(1)} \simeq 50$ Å, $L_c^{(2)} \simeq 100$ Å) in the infinite cut-off criteria (Fig.3(d)). In a bent rod, there are more non-bonded interactions, than in a straight one, as the proximity between non-neighbors increases. In longer rods, there are more such non-bonded interactions, and these introduce a buckling instability. Since with an infinite cut-off distance, we consider more such non-bonded interactions, $L_c^{(n)}$ is shorter than that calculated with a cut-off distance of 12 Å.

b. Coiled coils

$K_b^{(n)}$ of coiled coils with leucine zipper periodicity calculated using NMA or SMD, is higher than previously observed bending stiffness for coiled coils [9] [16]. This is because the close packing of apolar side chains, the intrahelical and interhelical interactions between side chains and a strong adherence of the leucine zipper sequence to the heptad pattern [24] make these coiled coils stiffer than those with non-heptad inserts in their sequence that were considered in those previous studies.

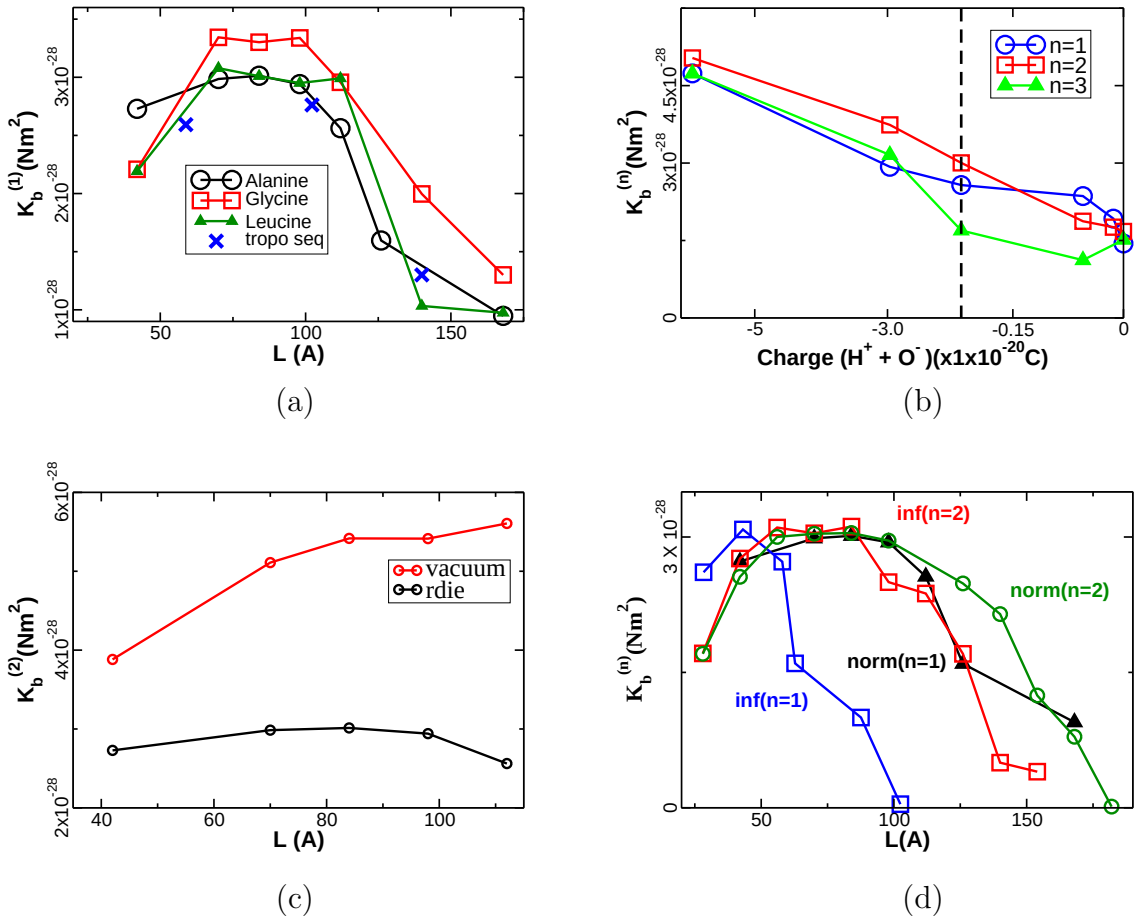

Fig. 3. Bending stiffness of α-helices. $K_b^{(n)}$ is the bending stiffness at the n-th bending mode and L is the length of the helix. (a) Alpha helices are relatively independent of their sequence composition. Considered here are helices composed of alanine, glycine, leucine and of sequences from a single helical chain in a two stranded tropomyosin molecule in RDIE. (b) Hydrogen bonding controls the stiffness of an α-helix. Even with a zero electrostatic force between the O^- & H^+ atoms, $K_b^{(n)}$ is about 1.441×10^{-28} Nm^2, indicating that the van der Waals interactions between these atoms and the non-bonded interactions between other atoms also contribute significantly towards the stiffness of the helix. Black dotted line shows the normal hydrogen bond strength. Region to the left of this signifies a stronger bond while weaker bonds lie to the right. (c) Alpha helices are softer in water simulating environment RDIE. (d) Typically, a cut-off distance of 12 Å is used in simulations, since interactions between atoms more than 12 Å away are considered negligible. When this cut-off distance is turned off and non-bonded interactions between all atoms are considered, $L_c^{(n)}$ is shorter ($\sim$ 50 Å for n=1, compared to $\sim$ 100 Å with a 12 Å cut off).

1. NMA: For coiled coils with leucine zipper periodicity, in the rise phase of the bending stiffness curve, $K_b^{(1)}$ is seen to increase from 0.928×10^{-27} Nm^2 for a rod of 39.702 Å (size of naturally occurring leucine zipper) to 1.887×10^{-27} Nm^2 for a rod of 162.360 Å. This is also marked as the start of the horizontal phase, where $K_b^{(1)}$ is seen to vary in the range of $(1.887 - 2.103) \times 10^{-27}$ Nm^2. The longest coiled coil considered is 326.38 Å, which has a $K_b^{(1)} \simeq 1.890 \times 10^{-27}$ Nm^2 & $K_b^{(2)} \simeq 1.947 \times 10^{-27}$ Nm^2(Fig.4). The VIBRA command in CHARMM used to retrieve the vibrational frequencies of the bending modes for $K_b^{(n)}$ calculation failed for longer helices due to the number of atoms involved (a 326.38 Å coiled coil has 4988 atoms). Despite not seeing a drop in $K_b^{(n)}$ for the lengths considered, we attempted to determine an estimate of $L_c^{(1)}$ using Eqn. 2.2 (Ref. Sec. 2). $L_c^{(1)}$ for these coiled coils is about 695 Å (detailed discussion in the next section Ref. Sec. 2).

   To see how this value of $K_b^{(n)}$ compares with other coiled coils, we considered the myosin-S2 domain and cortexillin. $K_b^{(1)}$ of cortexillin, a naturally occurring actin bundling protein of 145.81 Å is about 1.759×10^{-27} Nm^2. Myosin S2, being an unstable coiled coil is a bent rod. To minimize errors associated with length calculations, and since the equations from wave theory of rods (Eqn. 2.1, Eqn. 2.2) are not described well for bent rods, we used the sequence of myosin S2 (from the PDB:1NKN) to construct a straight coiled coil using Offer's code. $K_b^{(1)}$ of this rod is calculated to be about 1.024×10^{-27} Nm^2. Previously, a study estimated Young's modulus of a hardened transmembrane coiled coil involved in signaling a ligand binding to be about 3×10^{10} J/m^3 ($K_b^{(1)} \simeq 1.245 \times 10^{-27}$Nm^2 when the major helix radius is 5 Å [32]). These values of $K_b^{(n)}$ all lie in the rise phase of the bending stiffness curve (Fig. 4), indicating that the technique of

calculating $K_b^{(n)}$ using NMA by itself is accurate. It is the length scale of the rods that introduces the measured difference in $K_b^{(n)}$.

As already seen with α-helices, shorter coiled coils have a smaller measured $K_b^{(n)}$ due to the problems associated with a high aspect ratio and the end atoms non-bonded interactions. Also, a cylindrical description of helical rods suffers from errors associated with length estimations. The deviation of the measured length from the true length of the cylindrical rods minimizes as the rods become longer. Since, cylindrical description for helical coiled coils is towards application of wave theory of rods for calculating mechanical properties, there is no "right" way of determining true length of such systems. As this error cannot be avoided, it is better to consider longer rods for calculations (within the $L_c^{(n)}$ limit).

2. SMD:

Slope of the force displacement curve for a 162.36 $\mathring{A}$ coiled coils is about 0.0862 pN/Å. $K_b^{(1)}$ calculated using Eqn. 2.7 is about $(1.229 \pm 0.231) \times 10^{-27}$ Nm^2. For a 244.82 Å coiled coil, the slope is 0.03496 pN/Å, which translates to a $K_b^{(1)}$ of $(1.221 \pm 0.301) \times 10^{-27}$ Nm^2. This is less than $K_b^{(1)}$ calculated using NMA by about 35% (1.887×10^{-27} Nm^2 for 162.36 Å coiled coil and 1.999×10^{-27} Nm^2 for 244.82 Å coiled coil). Difference of about 35% between $K_b^{(1)}$ from NMA and SMD which was also observed in an earlier study that characterized bending stiffness of myosin S2 rod domain [9] could be due to the errors related to the estimation of an equilibrium position of the C-terminal tip upon displacement by the transverse force. Also, the applied forces could be greater than what the coiled coils can sustain as a homogeneous rod, thus making them appear softer than they actually are. More data points and longer simulations could elucidate this further.

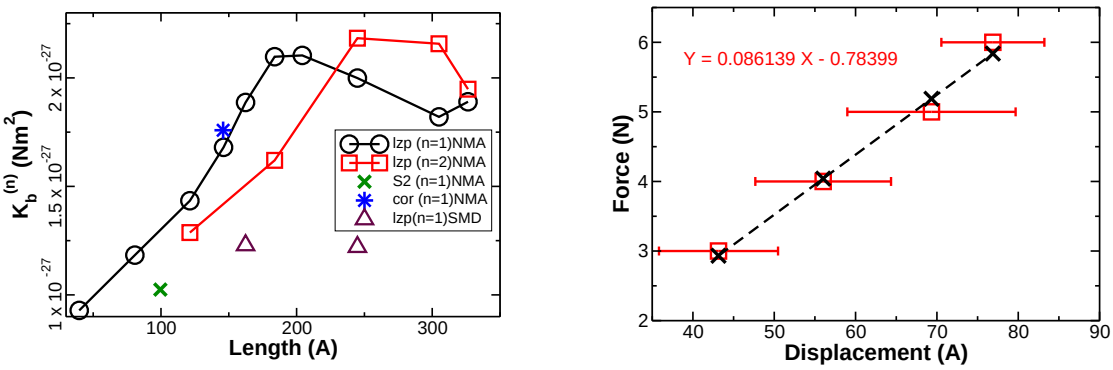

(a) (b)

Fig. 4. Bending stiffness of coiled coils. (a) $K_b^{(n)}$ is the bending stiffness at mode n. lzp stands for coiled coils with leucine zipper periodicity, S2 represents the stiffness of myosin S2 rod domain, built as a straight rod using sequence information from PDB:1NKN. Cortexillin is an actin bundling coiled coil with 101 residues per chain. (b) Force displacement curve for a 163 Å leucine zipper coiled coil. From the slope of (0.086 ± 0.007) pN/Å, $K_b^{(1)} \simeq (1.229 \pm 0.231) \times 10^{-27}$ Nm^2.

c. 1-D chain model

Bending stiffness of a 1D linear chain of beads (atoms) is calculated using both NMA and TMA. Since the charge of the individual beads is set to 0, the only non-bonded forces that exist are those due to Lennard-Jones potential(V_{LJ}) between the beads separated by a distance r,

$$V_{LJ}(r) = \epsilon[(\frac{r_{min}}{r})^{12} - 2(\frac{r_{min}}{r})^{6}] \tag{3.1}$$

where, r_{min} is the van der Waals radius (Å). When the two atoms are seperated by r_{min}, $V_{LJ} = \epsilon$. Hence, ϵ, characterizes the depth of the potential well (kcal/mol). Here, we vary the non-bonded interactions between atoms by varying ϵ and understand its effect on buckling instability.

1. NMA: The bending stiffness curve is plotted by plugging in vibrational frequencies of the first and second bending modes of chains of different lengths

into Eqn. 2.1. Like α-helices and coiled coils, this curve tracing $K_b^{(n)}$ for the 1-D chain is a horizontal line for a limited length scale, when ϵ of each atom was set to that of a carbon atom($\epsilon = 0.12$). Increasing ϵ, resulted in bending stiffness curves, where $K_b^{(n)}$ dropped at much shorter length scales. Non-bonded forces hence have a reciprocal relationship with $L_c^{(n)}$. Importantly, when ϵ is 0 kcal/mol, bending stiffness curve stays a horizontal line, irrespective of the length scale of the chain (Fig.5(a)). This is hence a strong evidence that shows that indeed inherent non-bonded forces along the length of a rod introduce a buckling instability.

2. TMA: The chain was subjected to thermal motion at 300K, and using the time averaged distance between the two end atoms, L_p was calculated from Eqn. 2.4. Since $L_p = \frac{K_b}{kT}$, variation of L_p with L, is a representative of the bending stiffness curve. For a non-zero ϵ, this curve tracing L_p at different lengths,L, recorded a drop similar to that observed when $K_b^{(n)}$ is calculated using NMA (about 75 Å in each case)(Fig. 5(b)). When L_p, is calculated using the distance between the first and middle atoms in the chain (instead of distance between the end atoms), it still drops beyond $L_c^{(1)}$, reiterating that increased non-bonded interactions during bending introduces the buckling instability.

2. Critical buckling length

From the bending stiffness curves of α-helices, coiled coils and 1-D chains, $L_c^{(n)}$ is identified as the point where $K_b^{(n)}$ drops (end of the horizontal region). At a resolution of about 10 Å, $L_c^{(n)}$ cannot be accurately determined from these bending stiffness curves. Hence, using Eqn. 2.2, we plot a straight line with $X = \frac{1}{L^2}$ vs $Y = \omega_n^2 L^2$. $K_b^{(n)}$ can be retrieved from the slope of this straight line ($\frac{K_b^{(n)}(c^{(n)})^4}{\rho_l}$) and F_{nb} from

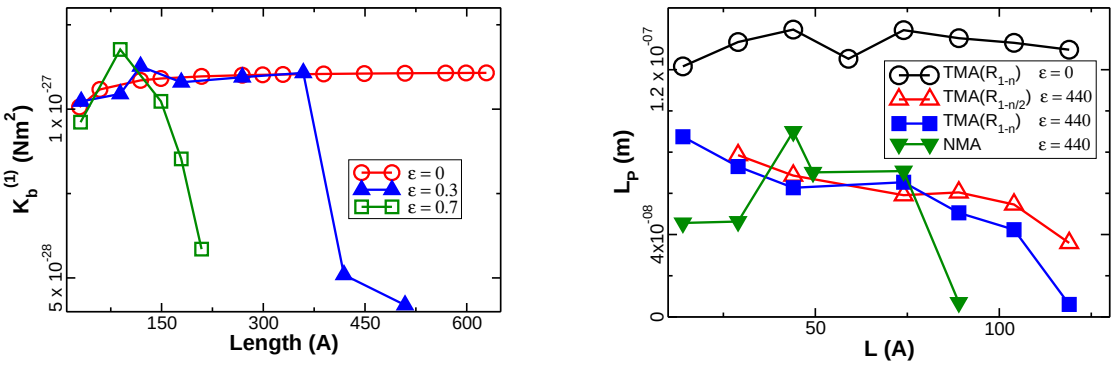

(a) (b)

Fig. 5. Critical buckling length has an inverse relationship with the non-bonded forces. (a) 1-D chain with bond stretching force constant K_{bond} = 8000 kcal/molÅ^2 and a bond angular force constant K_θ = 800 kcal/mol rad^2. $K_b^{(1)}$ dropped for shorter chains on increasing ϵ. There is no drop in $K_b^{(n)}$ for chains with atoms having zero ϵ. (b) 1-D chain with K_{bond} = 4000 kcal/molÅ^2 and K_θ = 400 kCal/mol. The persistence length (L_p) is calculated from the thermal fluctuations of the WLC. A very high ϵ (440) is used since the time scale over which the vector (R_{1-n} for end to end distance and $R_{1-n/2}$ for distance between an end atom and an atom at the center of the chain) becomes zero, is extremely high for long chains (For a chain of 120 Å, this was about 150 ns). TMA and NMA results are comparable, with both recording a drop in $K_b^{(1)}$ at about the same length ($\sim$ 75 Å).

the abscissa (constant of the straight line would be $\frac{F_{nb}(c^{(n)})^2}{\rho_l}$). $L_c^{(n)}$ is then calculated applying F_{nb} and $K_b^{(n)}$ into Eqn. 2.3.

The $X-Y$ plots are significant, as apart from a more accurate characterization of $L_c(n)$, we also get a representative $K_b^{(n)}$ (The bending stiffness curve can only give a range from the approximately horizontal line tracing $K_b^{(n)}$ for different sizes of the structure). To retrieve the slope and abscissa, we did not use data points from the initial rise phase of the bending stiffness curves. Results of these $X-Y$ plots for each of the structures are discussed below.

a. Alpha-helix

For a poly-alanine α-helix, from the slope of the $X-Y$ plots, $K_b^{(1)} = (2.985 \pm 0.080) \times 10^{-28}$ Nm^2 and $K_b^{(2)} = (3.180 \pm 0.0078) \times 10^{-28}$ Nm^2. From the abscissa of mode 1, $F_{nb} = 50.239 \pm 2.59$ pN, while from mode 2, $F_{nb} = 42.607 \pm 6.9136$ pN (Fig. 6(a)). $L_c^{(1)}$ is then determined to be 115.321 ± 2.867 Å. From the second mode, $L_c^{(2)} = 214.530 \pm 15.542$ Å. $L_c^{(1)}$ is about 93.910 ± 3.214 Å for a poly-glycine and 126.62 ± 4.318 Å for poly-leucine α-helices. These values of $L_c^{(n)}$ are comparable to the point of drop in $K_b^{(n)}$ in the bending stiffness curves (Fig. 3(a)).

b. Coiled coils

Despite not observing a drop in $K_b^{(n)}$ in the length scales of coiled coils used, we decided to plot the $X-Y$ plots, which yielded $L_c^{(1)} = 695.073 \pm 44.750$ Å and a $L_c^{(2)} = 1445.113 \pm 750.321$ Å. Such a high error region stems from the limitation in the length scales that can be explored using VIBRA and hence the number of data points that can be used in the analysis. Leucine zipper coiled coils of 700 Å have about 10,600 atoms and determining vibrational frequencies from VIBRA of CHARMM for such a big system becomes unviable.

c. 1-D chain model

From the $X-Y$ plots of a 1-D linear chain in Fig. 6(c), $K_b^{(1)} = (1.046 \pm 0.007) \times 10^{-27}$ Nm^2 and $K_b^{(2)} = (1.066 \pm 0.0001) \times 10^{-27}$ Nm^2. From the abscissa of mode 1, $F_{nb} = 2.756 \pm 0.090$ pN, while from the abscissa of mode 2, $F_{nb} = 1.995 \pm 0.091$ pN. Non-bonded force measured using CHARMM command SCALAR DX on this 1-D chain in an energy minimized condition is about 3 pN. Similarly, for the 1-D linear chain with a bending stiffness of about $4.163 \times 10^{-27} Nm^2$ (Ref. Fig. 5(b)), F_{nb} from $X-Y$ plots is about 7.3 pN, while that calculated using CHARMM is about 10 pN. Further, when the non-bonded forces within the system are turned off, F_{nb} from the $X-Y$ plots is 0 ± 0.0065 pN.

For α-helices and coiled coils, $L_c^{(1)} < L_p$ (in a poly-alanine α-helix, $L_c^{(1)} = 115.321 \pm 2.867$ Å, while $L_p \simeq 740.342 \pm 19.239$ Å). When 1-D chains were built to have a stiffness such that $L_c^{(1)}$ is greater than L_p, then F_{nb} from the $X-Y$ plots was about 50-100 times lesser than the non-bonded forces measured using SCALAR DX command. Since NMA assumes a harmonic behavior of the system, when determining vibrational frequencies, the deviation between the natural vibrational frequency and that measured using CHARMM becomes significant with higher non-bonded forces. This introduces the error in the measurements.

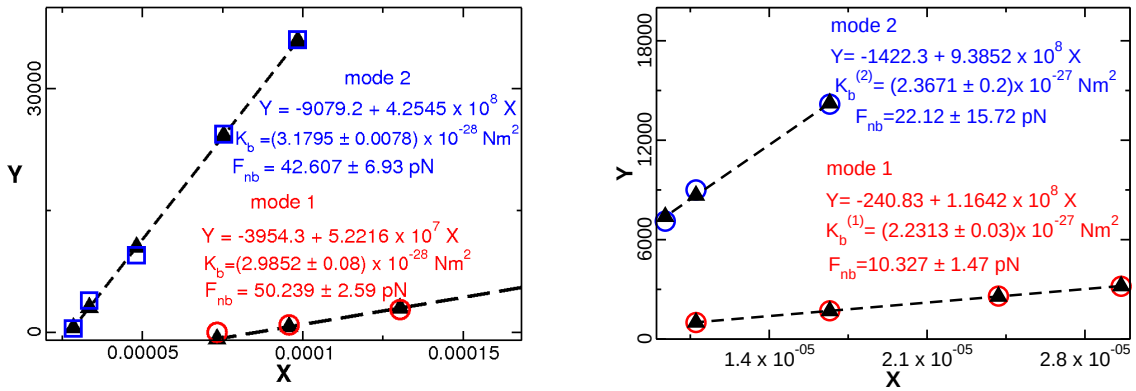

(a)

(b)

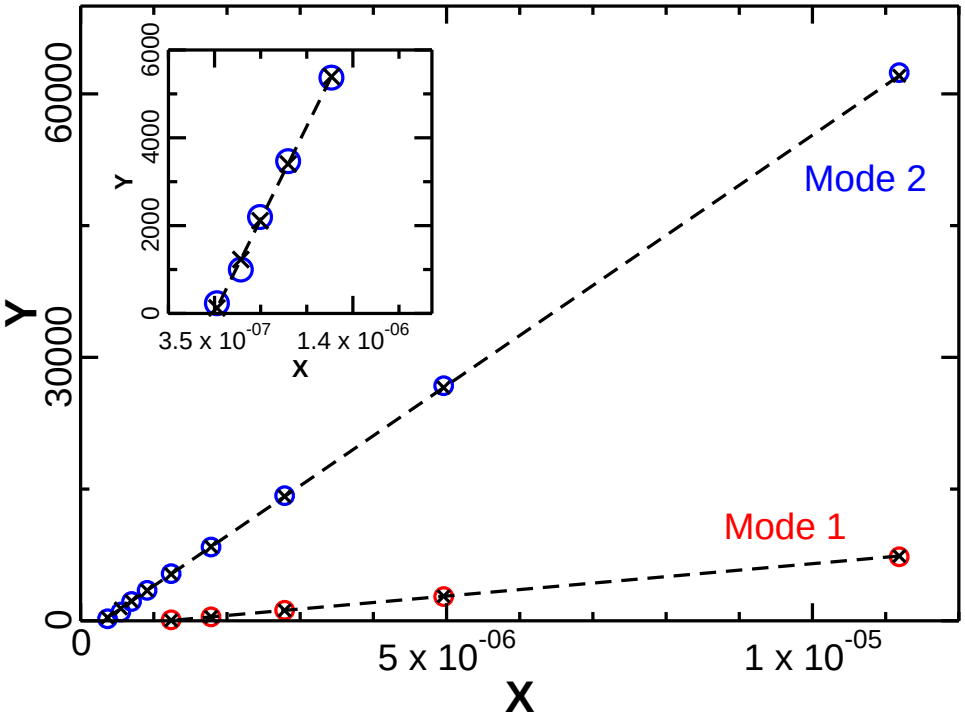

(c)

Fig. 6. Critical buckling length from X-Y plots. $X = \frac{1}{L^2}$ and $Y = \omega_n^2 L^2$. (a) Poly-alanine α-helix. (b)Coiled coils with leucine zipper peridicity. (c) 1-D chain with $K_{bond} = 8000$ kcal/molÅ^2 and $K_\theta = 800$ kCal/mol rad^2. Since X, Y vary over a large scale (X varies from 3.5×10^{-7} to 1×10^{-5}), we show only the regions involving large L (small X) for the α-helices and coiled coils (like the inset for the 1-D chains).

CHAPTER IV

DISCUSSION AND CONCLUSION

Within the horizontal phase of the bending stiffness curve, $K_b^{(n)}$ of α-helices calculated using NMA is nearly independent of the amino-acid composition and varies between $2.985 \times 10^{-28} - 3.356 \times 10^{-28}$ Nm^2. Sequence independence shows that hydrogen bonding between the N-H of i-th and C=O of the $(i+4)$-th amino-acids controls the stiffness of α-helices. In the absence of electrostatic force in the hydrogen bonding, bending stiffness is about 1.441×10^{-28} Nm^2. This shows that the van der Waals interactions between the H and O atoms (of the N-H,C=O network) and non-bonded interactions between other atoms contribute significantly towards the stiffness of the helix. Contributions by non-bonded interactions between other atoms towards the stiffness is reiterated by the fact that helices were softer in the water simulating RDIE environment ($K_b^{(1)} \simeq (3.107 - 3.210) \times 10^{-28}$ Nm^2 Vs. $\simeq (5.109 - 5.606) \times 10^{-28}$ Nm^2 in vacuum for a poly-alanine helix).

Since most of the previous computational and experimental studies that characterized their mechanical properties considered α-helices with length less than this critical buckling length limit, their assumption of linear elasticity stayed valid. Within this limited length scale, bending stiffness retrieved using a triad system that follows its local curvature [8] will fail to capture the effect of non-bonded interactions on the whole system. Filaments with hydrogen-bonding have been observed to be anisotropic, being nearly inextensible in the longitudinal direction [17]. Hence, calculating Youngs modulus from the stretching characteristics using an Atomic Force Microscope [7], would make α-helices appear much stiffer. Despite having a persistence length of about 760 Å (for a poly-Alanine α-helix from $K_b^{(n)}$ in RDIE, L_p is about 740.342 ± 19.239 Å), isolated α-helices associated with mechanical roles have a length

that is less than or about 115 Å [3] [33]. We believe that apart from their functional significance, with $L_c^{(1)}$ in this range (for poly-Alanine α-helix, $L_c^{(1)}$ is 115.321 ± 2.867 Å), α-helices are designed to stay within this limit in order to avoid the predominance of non-bonded forces seen at lengths greater than $L_c^{(n)}$.

From NMA and SMD calculations, coiled coils with leucine zipper periodicity have a $K_b^{(1)}$ of about $(2.231 \pm 0.030) \times 10^{-27}$ Nm^2 and $L_c^{(1)} = 695.073 \pm 44.750$ Å. $K_b^{(1)}$ is higher than previously calculated values [9] [16] due to the stiffness offered by tight knob into hole packing in a leucine zipper periodicity. Bending stiffness of an S2 rod domain was estimated to be about 0.720×10^{-27} Nm^2 [9]. However, S2 rod domain is an unstable coiled coil, with absence of some of the interhelical salt bridge formations [34]. Further, from the crystal structure (PDB:1NKN), the rod domain is bent about the cylindrical axis. Estimating its length by considering them as straight cylinders would result in a smaller $K_b^{(n)}$. To avoid these length associated errors, we built a straight coiled coil using the sequence information from the crystal structure (PDB:1NKN) and the $K_b^{(1)}$ for such a structure is about 1.025×10^{-27} Nm^2.

Long coiled coils such as tropomyosin, with its alanine staggers, breaks in the heptad periodicity and naturally bent shape [26] and Rad50 (a DNA repair protein) cannot be considered as a single coiled coil when determining its bending stiffness [35]. Each region (N-terminal, C-terminal and central rod domain) are bound to have different stiffnesses by virtue of their composition and it would be difficult to arrive at a single representative stiffness constant for the whole molecule. Our estimate of $K_b^{(1)}$ for coiled coils using leucine zipper may be an upper limit (when trying to arrive at bending stiffness of coiled coils in general), as naturally occurring coiled coils usually have some breaks in the heptad periodicity along their length, and this would affect the stiffness.

Since the drop in bending stiffness due to the intrinsic non-bonded forces is

not restricted to only α-helices and coiles coils, but is seen even in the 1-D linear chains, it would be relevant and important to characterize $L_c^{(n)}$ for naturally occurring filamentous proteins. While their linear response to bending is characterized by $K_b^{(n)}$ and L_p, determining $L_c^{(n)}$ for α-helices, coiled coils and filaments in nature would give a complete picture when modeling the mechanical behavior of such systems.

REFERENCES

[1] L. Pauling, R. Corey, and H. Branson, "The Structure of Proteins: Two Hydrogen-Bonded Helical Configurations of the Polypeptide Chain," *Proceedings of the National Academy of Sciences of the United States of America*, vol. 37, no. 4, pp. 205–211, 1951.

[2] F. Crick, "The packing of alpha helices: Simple coiled coils," *Acta Crystallographica*, vol. 365, p. 110X, 1953.

[3] X. Chen, D. Tomchick, E. Kovrigin, D. Arac, M. Machius, T. Sudhof, and J. Rizo, "Three-dimensional structure of the complexin/snare complex," *Neuron*, vol. 33, pp. 397–409, 2002.

[4] J. Jaud, F. Bathe, M. Schliwa, M. Rief, and G. Woehlkey, "Flexibility of the neck domain enhances kinesin-1 motility under load," *Biophysical Journal*, vol. 91, pp. 1407–1412, August 2006.

[5] J. Brown and C. Cohen, "Regulation of muscle contraction by tropomyosin and troponin: How structure illuminates function," *Advances in Protein Chemistry*, vol. 71, pp. 121–159, 2005.

[6] G. Bao and S. Suresh, "Cell and molecular mechanics of biological materials," *Nature*, vol. 2, pp. 715–725, NOV 2003.

[7] A. Idiris, M. T. Alam, and A. Ikai, "Spring mechanics of α-helical polypeptide," *Protein Engineering*, vol. 13, no. 11, pp. 763–770, 2000.

[8] S. Choe and S. X. Sun, "The elasticity of α-helices," *Journal of Chemical Physics*, vol. 122, no. 244912, pp. 244 912–1–9, 2005.

[9] I. Adamovic, S. Mijailovich, and M. Karplus, "The Elastic Properties of the Structurally Characterized Myosin II S2 Sub-domain: A Molecular Dynamics and Normal Mode Analysis," *Biophysical Journal*, 2008.

[10] Y. Suezaki and N. Go, "Fluctuations and mechanical strength of α-helices of polyglycine and poly(l-alanine)," *Biopolymers*, vol. 15, p. 2137, 1976.

[11] M. Lantz, S. Jarvis, H. Tokumoto, T. Martynski, T. Kusumi, C. Nakamura, and J. Miyake, "Stretching the alpha-helix: a direct measure of the hydrogen-bond energy of a single-peptide molecule," *Chemical Physics Letters*, vol. 315, pp. 61–68, 1999.

[12] J. Ireta, J. Neugebauer, M. Scheffler, A. Rojo, and M. Galvan, "Density functional theory study of the cooperativity of hydrogen bonds in finite and infinite alpha-helices," *Journal of Physical Chemistry B*, vol. 107, pp. 1432–1437, 2003.

[13] D. Lee, S. Ivaninskii, P. Burkhard, and R. Hodges, "Unique stabilizing interactions identified in the two-stranded alpha-helical coiled-coil: Crystal structure of a cortexillin i/gcn4 hybrid coiled-coil peptide," *Protein Science*, vol. 12, pp. 1395–1405, 2003.

[14] A. Pineiro, A. Villa, T. Vagt, B. Koksch, and A. Mark, "A molecular dynamics study of the formation, stability, and oligomerization state of two designed coiled coils:possibilities and limitations," *Biophysical Journal*, vol. 89, pp. 3701–3713, December 2005.

[15] Y. Yu, O. Monera, R. Hodges, and P. L. Privalov, "Ion pairs significantly stabilize coiled-coils in the absence of electrolyte," *Journal of Molecular Biology*, vol. 255, pp. 367–372, 1996.

[16] S. Hvidt, F. H. M. Nestler, M. L. Greaser, and J. D. Ferry, "Flexibility of myosin rod determined from dilute solution viscoelastic measurements," *Biochemistry*, vol. 21, pp. 4064–4073, 1982.

[17] J. Park, B. Kahng, R. D. Kamm, and W. Hwang, "Atomistic simulation approach to a continuum description of self-assembled β-sheet filaments," *Biophysics Journal*, vol. 90, pp. 2510–2524, 2006.

[18] L. Landau and E. Lifshitz, *Course of Theoretical Physics, Vol. 7: Theory of Elasticity.* Nauka, Moscow, 1987.

[19] J. Howard, *Mechanics of Motor Proteins and the Cytoskeleton.* Sunderland, MA: Sinauer, 2001.

[20] W. Humphrey, A.Dalke, and K.Schulten, "Vmd:visual molecular dynamics," *Journal of Molecular Graphics*, vol. 14, no. 1, p. 33, 1996.

[21] I. Abbreviations, "Symbols for the description of the conformation of polypeptide chains. Tentative rules (1969). IUPACIUB Commission on Biochemical Nomenclature," *Biochemistry*, vol. 9, pp. 3471–3479, 1970.

[22] B. Brooks, R. Bruccoleri, B. Olafson, D. States, S. Swaminathan, and M. Karplus, "CHARMM: A program for macromolecular energy, minimization, and dynamics calculations," *Journal of Computational. Chemistry*, vol. 4, pp. 187–217, 1983.

[23] K. Itoh and T. Shimanouchi, "Vibrational frequencies and modes of α-helix," *Biopolymers*, vol. 9, p. 383, 1970.

[24] E. K. O'Shea, J. D. Klemm, P. S. Kim, and T. Alber, "X-ray structure of the gcn4 leucine zipper, a two-stranded, parallel coiled coil," *Science*, vol. 254, no.

5031, p. 539, 1991.

[25] G. Offer and R. Sessions, "Computer modelling of the alpha-helical coiled coil:packing of side-chains in the inner core," *Journal of Molecular Biology*, vol. 249, pp. 967–987, 1995.

[26] J. Brown, K. Kim, G. Jun, N. Greenfield, R. Dominguez, N. Volkmann, S. Hitchcock-DeGregori, and C. Cohen, "Deciphering the design of the tropomyosin molecule," *Proceedings of the National Academy of Sciences*, p. 131219198, 2001.

[27] P. Burkhard, R. A. Kammerer, M. O. Steinmetz, G. P. Bourenkov, and U. Aebi, "The coiled-coil trigger site of the rod domain of cortexillin i unveils a distinct network of interhelical and intrahelical salt bridges," *Structure*, vol. 8, pp. 223–230, 2000.

[28] M. Schaefer and M. Karplus, "A comprehensive analytical treatment of continuum electrostatics," *J Phys Chem*, vol. 100, pp. 1578–1599, 1996.

[29] R. D. Jr, "Comparative modeling of casp3 targets using psi-blast and scwrl," *Proteins: Structure, Function, Genetics*, vol. 3, pp. 81–87, 1999.

[30] T. Schlick, *Molecular Modeling and Simulation: An Interdisciplinary Guide*. Springer-Verlag, New York, 2002.

[31] A. Matsumoto and N. Go, "Dynamic properties of double-stranded dna by normal mode analysis," *Journal of Chemical Physics*, vol. 110, pp. 11 070–11 075, 1999.

[32] R. Hawkins and T. McLeish, "Dynamic allostery of protein alpha helical coiled coils," *Journal of Royal Society Interface*, vol. 3, no. 6, pp. 125–138, 2006.

[33] B. Kuhlman, H. Yang, J. Boice, R. Fairman, and D. Raleigh, "An exceptionally stable helix from the ribosomal protein L9: implications for protein folding and stability," *Journal of Molecular Biology*, vol. 270, no. 5, pp. 640–647, 1997.

[34] Y. Li, J. Brown, L. Reshetnikova, A. Blazsek, L. Farkas, L. Nyitray, and C. Cohen, "Visualization of an unstable coiled coil from the scallop myosin rod," *Nature*, vol. 424, pp. 341–345, JULY 2003.

[35] J. van Noort, T. van der Heijden, M. de Jager, C. Wyman, R. Kanaar, and C. Dekker, "The coiled-coil of the human Rad50 DNA repair protein contains specific segments of increased flexibility," *Proceedings of the National Academy of Sciences*, vol. 100, no. 13, p. 7581, 2003.

VITA

Sirish Kaushik Lakkaraju received his Bachelor of Engineering degree in Electronics and Instrumentation from the University of Madras at Chennai, India in 2003. He entered the Master of Science program in Biomedical Engineering at Texas A&M University in September 2005. His research interests include molecular biomechanics, focusing on α helices, coiled coils and filamentous proteins.

Mr.Lakkaraju maybe reached at the Department of Biomedical Engineering, 337 Zachry Engineering Center, 3120 TAMU, College Station, TX 77843-3120. His email is kaushik.lakkaraju@gmail.com